Vibrational - Electrical Properties Relationship in Donor Doped TiO_2 by Raman Spectroscopy

Journal:	*The Journal of Physical Chemistry*
Manuscript ID	jp-2016-052824.R2
Manuscript Type:	Article
Date Submitted by the Author:	27-Jul-2016
Complete List of Authors:	Mazzolini, Piero; Politecnico di Milano, Russo, Valeria; Politecnico di Milano, Department of Energy Casari, Carlo Spartaco; Politecnico di Milano, Department of Energy Hitosugi, Taro; Tohoku University, Advanced Institute for Materials Research Nakao, Shoichiro; Kanagawa Academy of Science and Technology (KAST) Hasegawa, Tetsuya; Univ.Tokyo, Chemistry Li Bassi, Andrea; Politecnico di Milano, Department of Energy

Vibrational - Electrical Properties Relationship in Donor Doped TiO_2 by Raman Spectroscopy

P. Mazzolini, [1,2] *V. Russo,* [1]* *C.S. Casari,* [1,2] *T. Hitosugi,* [3] *S. Nakao,* [3] *T. Hasegawa,* [3] *A. Li Bassi* [1,2]

[1] Department of Energy - Politecnico di Milano, via Ponzio 34/3, I-20133 Milano, Italy

[2] Center for Nano Science and Technology - IIT@PoliMI, Via Pascoli 70/3, I-20133 Milano, Italy

[3] Kanagawa Academy of Science and Technology (KAST), Kawasaki 213-0012, Japan

* To whom correspondence should be addressed. E-mail: valeria.russo@polimi.it; tel. +390223996364

Abstract

Transparent conducting TiO_2, obtained by Nb or Ta doping of the anatase structure, is gaining increasing attention for the development of transparent electrodes. Usually, regardless the deposition technique, a crystallization process in reducing atmosphere is necessary to achieve large mobility; in addition, electrical and optical properties are also strongly sensitive to the oxygen deposition pressure. These facts reveal that the defect chemistry of donor doped TiO_2 is not trivial and involves a strict interplay among extrinsic dopant atoms, oxygen vacancies and 'electron killer' defects such as Ti vacancies and O interstitials.

We here present a Raman characterization of donor-doped TiO_2 films synthesized under several deposition and post-annealing conditions, employing different doping levels and dopant elements (*i.e.* Ta and Nb). Correlations between structure, crystallinity, shift and width of Raman peaks and electrical properties are shown and discussed. In particular, a clear relationship between the shift of the $E_g(1)$ anatase Raman mode and the charge carrier density is found, while the $B_{1g}(1)$ mode connected to Ti-Ti vibrations is significantly affected by the extrinsic doping level. In this complex framework Raman spectroscopy can provide an invaluable contribution towards understanding the material structure and its influence on the functional properties.

1. Introduction

Titanium dioxide is a very well-known and widely studied material for several energy-related applications like photovoltaics, photocatalytic water splitting, lithium ion batteries and fuel cells.[1] It mainly occurs in two crystalline forms, the stable rutile and the metastable anatase phase; both structures are characterized by a wide energy bandgap (E_g ~ 3 eV for rutile and E_g ~ 3.2 eV for anatase).[2] In new generation photovoltaic devices (e.g. Dye-Sensitized Solar Cells - DSSCs, perovskite solar cells, organic-inorganic hybrid solar cells) anatase TiO_2 is usually employed as an electron selective layer or as nanoporous photoanode.[3,4]

In 2005 the capability to increase the conductivity of this wide bandgap semiconductor was demonstrated, making it suitable for transparent conducting applications, by replacing a certain amount of Ti atoms (around 5 at.%) inside the anatase cell with group V elements like Nb or Ta (TNO and TaTO respectively).[5,6] This results in a significant increase of the charge carrier density of doped TiO_2 thin films (up to ~ 10^{21} cm^{-3}), both in the form of single crystal (by epitaxial growth on single crystal substrates via a one-step high temperature deposition process) as well as polycrystalline film (on cheap substrates via room temperature deposition followed by an *ex-situ* crystallization process).[7] However, the obtainment of transparent conductive properties is strictly related to oxygen-poor conditions (deposition and/or post-deposition thermal treatment, e.g. annealing in vacuum); this evidence still represents an open and debated point in the fundamental understanding of the physical mechanisms determining the electrical transport properties of these materials.[8-14] Some of us have experimentally demonstrated the possibility of finely tuning the charge carrier density of TaTO polycrystalline films in a wide range (10^{19} cm^{-3} < n < 10^{21} cm^{-3}), just slightly changing the oxygen partial pressure during the room temperature pulsed laser deposition (PLD) process, when followed by post-crystallization in vacuum.[8] Moreover, it was also demonstrated that in TiO_2-based films oxygen incorporation from the

crystallization environment can directly or indirectly play a detrimental role with respect to the electrical properties; O incorporation can however be eluded via Ultra-Fast-Annealing treatments (UFA) which limit oxygen exchange with the atmosphere even under non-reducing conditions (N_2-based atmosphere).[15] These facts point to the possibility to rule the formation/annihilation of a large amount of charged defects (e.g. tantalum substitutional Ta_{Ti} atoms, oxygen vacancies V_O, and 'electron killer' defects such as oxygen interstitials O_i, titanium vacancies V_{Ti}) in the anatase lattice and reveal a strict but non trivial interplay between extrinsic and intrinsic defects. In support of this assumption, a clear connection was found between synthesis conditions and the crystal lattice parameters of doped TiO_2 films.[8] It is thus plausible to assume that the vibrational properties of the anatase lattice are affected as well, as a function of a different amount of extrinsic and intrinsic dopants/defects, although in a non-obvious way.

Within this complex framework, Raman spectroscopy represents an important tool towards understanding the material structure and its influence on the functional properties. It is based on the inelastic scattering of light by phonons, with the fundamental mediation of electrons, and is therefore useful to investigate structure, electronic properties and electron-phonon interaction, as we have already demonstrated for some oxides and semiconductor materials.[16,17] This aspect is particularly interesting for TiO_2-based transparent conducting oxides (TCO) when doping effects are investigated. In this work we present a detailed Raman characterization of polycrystalline TiO_2 thin films doped with both Ta and Nb, when varying the doping level and the deposition/annealing environment, with the aim to investigate in a systematic way the relationship between vibrational and electrical properties. In particular we underline a clear and interesting correlation between the shift of the $E_g(1)$ anatase Raman vibrational mode and the charge carrier density which is found to be independent on the nominal extrinsic dopant amount and on the donor element employed.

2. Experimental Section

Thin films of Ta-doped TiO_2 (Ta:TiO_2 or TaTO) and Nb-doped TiO_2 (Nb:TiO_2 or TNO) have been synthesized by physical vapor deposition techniques and investigated, including undoped TiO_2 for comparison. TiO_2 and Ta:TiO_2 (TaTO) thin films (typically about 150 nm thick) with different doping amount (in the following 'Ta content', nominally 1%, 5% and 10% at.) have been deposited by Pulsed Laser Deposition (PLD) on soda-lime glass substrates at room temperature using a lamp-pumped Q-switched Nd:YAG pulsed laser (4th harmonic, λ = 266 nm, repetition rate f_p = 10 Hz, pulse duration ~ 6 ns, target-to-substrate distance = 50 mm). TaTO films with 1% Ta content have been obtained using a TiO_2 target (powder purity 99.9%) partially covered (~ 1% of the surface) with Ta-metallic wires. TiO_2 films were obtained starting from the same ceramic target, while TaTO with 5% and 10% Ta content were obtained ablating sintered Ta_2O_5:TiO_2 (molar ratio of 0.025:0.975 and 0.05:0.95 respectively, powders purity 99.99 %) targets. Different oxygen partial pressures (p_{O2} in the range of 0.9 – 2.25 Pa) and laser fluences (in the range of 0.9 – 3 J/cm^2) have been used to tune the film properties. The PLD process was always followed by an ex-situ annealing treatment performed in different atmospheres (vacuum - $p < 4\times10^{-5}$ Pa, Ar / H_2 mixture with H_2 at 2 - 3%, N_2 or air at ambient pressure) at different temperatures (450°C, 460 °C, 500°C and 550°C) with different dwell times (0, 10 and 60 minutes), in home-made heating systems. In the following we will refer to a thermal treatment with 60 minutes dwell time at 550°C and slow heating/cooling ramp of 10 K min^{-1} as '*standard annealing*' and to a thermal treatment without (*i.e.* zero) dwell time, peak temperature of 460 °C and heating/cooling ramps up to 300 K min^{-1} as '*ultra-fast annealing*' (UFA).[8, 15] Nb-doped TiO_2 thin films with 5% at. Nb content (NTO) on soda lime glass substrates were obtained by sputtering deposition. Ar pressure and p_{O2} during depositions were 1 Pa and 3×10^{-4} – 1×10^{-3} Pa, respectively. As in the case of TaTO films, amorphous films were deposited at room temperature, followed by an ex-situ vacuum annealing

process in a commercial furnace (ULVAC RIKO, MILA-5000) to crystallize the films into anatase phase. Annealing temperature and pressure during annealing were 450 °C and 1×10^{-3} Pa, respectively. Micro-Raman measurements were performed with a Renishaw In Via spectrometer with Ar^+ laser, λ = 514.5 nm, power on sample below 1 mW, in order to avoid sample damage by the laser. In order to correctly determine the Raman mode position and width we performed Lorentzian fits on the analyzed peaks. The electrical properties were determined in 4-point probe configuration with a Keithley K2400 Source/Measure Unit as a current generator (from 100 nA to 10 mA), an Agilent 34970A voltage meter and a 0.57 T Ecopia permanent magnet.

3. Raman spectroscopy of TiO_2-based materials

The primitive unit cell of anatase contains two TiO_2 units (6 atoms), leading to 18 vibrational modes (15 optical and 3 acoustic). From factor group analysis (D_{4h}^{19} - $I4_1/amd$ space group) the optical modes at the Γ point (Γ_{opt}) can be classified as

$$\Gamma_{opt} = A_{1g} + A_{2u} + 2B_{1g} + B_{2u} + 3E_g + 2E_u$$

where the three A_{2u} and 2 E_u modes are IR active, the B_{2u} mode is silent, while six modes are Raman active, namely the A_{1g}, 2 B_{1g} and 3 E_g.[18,19] According to lattice dynamics studies, the doubly degenerate E_g modes involve atom displacements perpendicular to the *c*-axis, while for the other modes atoms move parallel to the c-axis.[18-20] Most of the modes are predicted to involve both Ti and O atom displacements, but the $B_{1g}(1)$ mode should be dominated by Ti atom motions and the A_{1g} mode is expected to be a pure oxygen vibration.[20-22] Calculated and experimentally measured positions of the 6 Raman peaks are well-known and largely reported in the literature,[17,19,23] with the following reference values: $E_g(1)$ at 144 cm^{-1}, $E_g(2)$ at 197 cm^{-1}, $B_{1g}(1)$ at 399 cm^{-1}, $B_{1g}(2)$ at 519 cm^{-1}, A_{1g} at 513 cm^{-1}, $E_g(3)$ at 638 cm^{-1}. The overlapping between $B_{1g}(2)$ and A_{1g} prevents the detection of the weaker A_{1g}

mode in unpolarized measurements at room temperature. On the contrary, at low temperature (5 K) the narrowing of the Raman lines allows to distinguish the two contributions.[20]

The $E_g(1)$ Raman peak at 144 cm^{-1} is the most intense and largely the most investigated in the literature. Several works focus on the variation of position, width and shape of this peak in relation to several effects: defects in the stoichiometry due to oxygen deficiency,[17,24] phonon confinement in nanoparticles,[17,25-28] extrinsic doping,[28-33] presence of minority phases,[32] pressure and temperature effects,[34] film thickness and influence of the substrates.[35] It is not straightforward to distinguish the influence of a single effect among the others, because they are often simultaneously present in the investigated sample. Moreover, according to the phonon band structure of anatase,[18] a shift towards higher wavenumbers is always expected for this peak when the fundamental Raman selection rule is relaxed under some disordering of the perfect crystalline structure, thus preventing an easy assignment of observed shifts to a specific effect. This aspect must be carefully taken into account when the $E_g(1)$ peak is analyzed. Especially when different effects coexist, the analysis of the other anatase Raman peaks can contain complementary information with respect to the peak at 144 cm^{-1}. Despite this fact, fewer papers focusing on the other Raman features are present.[25,34,35]

In this work some of the mentioned effects can be reasonably excluded. In fact, all the films crystallize in the anatase phase after annealing, with crystal grain size in the order of several micrometers in the horizontal direction, and limited by the film thickness in the vertical direction (typically 150 nm), as we have shown in our previous works also by means of X-ray diffraction (XRD) analysis;[8] this suggests that confinement effects, which are relevant below characteristic size of 10-15 nm, should not significantly affect the Raman spectrum.[17] Moreover, all films are deposited on the same substrate (soda lime glass) with comparable thickness. In addition to this the presence of minority phases, such as segregated Ta_2O_5 (in the case of Ta-doped films) or different TiO_2 polymorphs, like brookite or rutile, was never detected in the Raman spectrum of all the analyzed samples, nor by XRD.

We here focus on the influence of extrinsic doping, by varying the nominal Ta content from 1% to 10%, and of the defectivity related to oxygen stoichiometry, by tuning oxygen partial pressure during deposition and/or annealing. A detailed analysis of all the Raman features with respect to preparation details (deposition/annealing/doping) and functional properties (with particular attention to charge carrier density) allows us to provide new insights in the structure of doped TiO_2 TCOs.

4. Results and discussion

All as prepared films (*i.e.* deposited at room temperature) are characterized by the absence of a long range order. In fact, their Raman spectra show the presence of broad bands typical of amorphous/highly disordered titanium oxide. Films annealed at a temperature between 460 °C and 550 °C undergo a transition to polycrystalline anatase regardless of the dopant concentration (e.g. Ta = 0 – 10 at.%) and of the different deposition/annealing conditions (*e.g.* in air or in vacuum). In **Figure 1** representative Raman spectra before and after annealing are reported, clearly showing the evolution from amorphous to crystalline anatase.

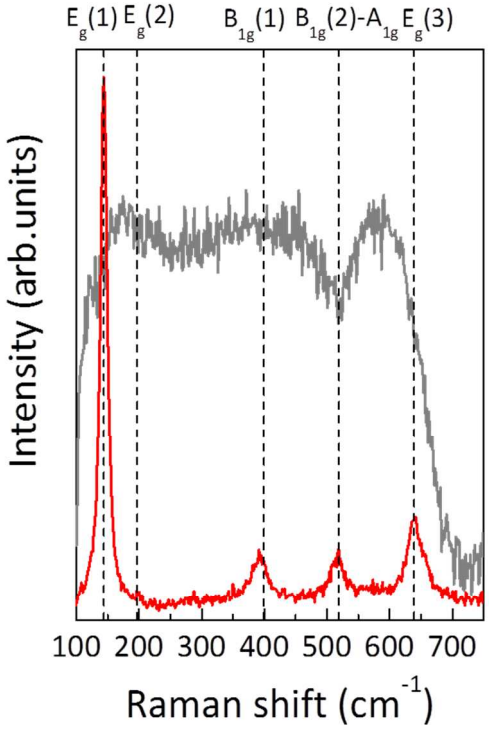

Figure 1. Raman spectra obtained for a film as deposited (with 1.25 Pa O_2) (grey curve) and after annealing in air at 550°C (red curve)

4.1 Effect of extrinsic dopant

We first focus on the role of Ta as Ti substitutional (Ta_{Ti}) in the anatase cell (*i.e.* extrinsic dopant). As discussed in the introduction, a post crystallization process in reducing atmosphere (*e.g.* vacuum) is the basic requirement to obtain highly conducting TiO_2-based thin films with a *standard* annealing cycle ($p < 4\times10^{-5}$ Pa; 60 minutes at 550°C, with heating/cooling ramp of 10 K min^{-1}).

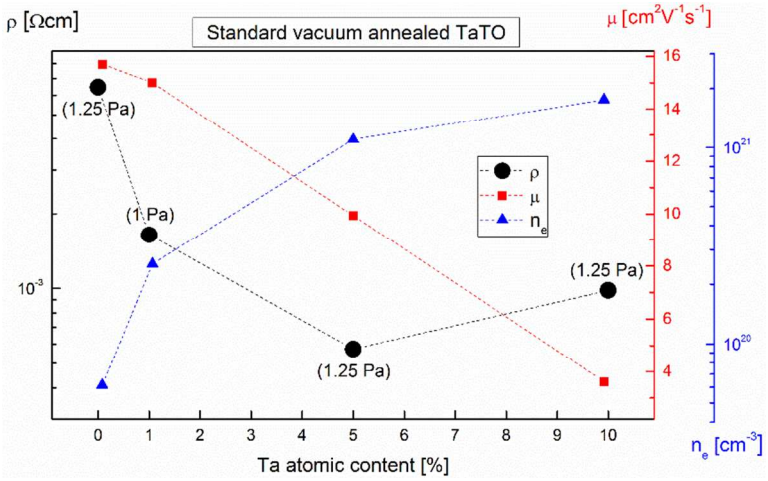

Figure 2. Best electrical properties obtained for standard vacuum annealed polycrystalline TaTO films as a function of different Ta content. The black circles represent the resistivity ρ, the blue triangles the charge carrier density n and the red squares the electron mobility μ. In the brackets the oxygen partial pressure employed during the previous room temperature deposition process is reported.

In **Figure 2** we report the optimal electrical properties obtained for vacuum annealed TiO_2 films deposited in optimal conditions (p_{O2} reported in the brackets), as a function of a different Ta content (*i.e.* extrinsic dopant). We notice that the measured charge carrier density of TaTO samples is in the same range of the Ta nominal content (triangles in Figure 2); this is due to the high dopant activation efficiency typical of TiO_2-based TCOs ($n = 10^{19}$ cm^{-3} – 10^{21} cm^{-3} for Ta ranging from 0 to 10 at.%).[6] Also the electron mobility is dependent on the Ta content (squares in Figure 2); this is most likely related to the increasing concentration of ionized impurities in the crystal lattice (*i.e.* Ta_{Ti}). The resulting resistivity (circles in Figure 2) decreases (starting from $\rho \sim 6 \times 10^{-3}$ Ωcm for undoped TiO_2) while increasing the Ta content up to 5 at.%. This defines the TaTO optimally doped composition (*i.e.* minimum recorded resistivity $\rho \sim 5 \times 10^{-4}$ Ωcm). For the overdoped composition (Ta content = 10 at.%), the decrease of the electron mobility prevails on the increment of n ($\rho \sim 1 \times 10^{-3}$ Ωcm). We

observe that the resistivity values and trends are very similar to the case of epitaxially grown TaTO thin films with different Ta content previously reported in the literature;[6] this highlights the limited impact on transport properties played by grain boundaries. Nonetheless, in agreement with previous reports,[8] an oxygen-rich crystallization annealing atmosphere (*e.g.* air) always results in electrically insulating films (not measurable with our experimental setup).

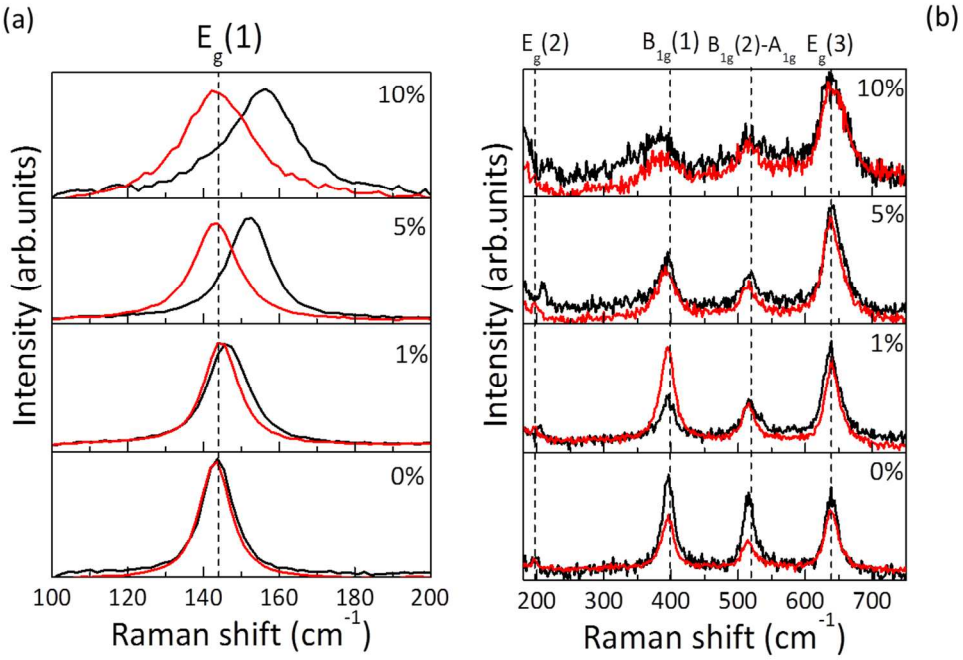

Figure 3. Raman spectra of TaTO films with different Ta content after standard vacuum annealing (black curves) or air annealing at 500°C (red curves). Vertical lines indicate reference peak position for anatase crystal.

In **Figure 3** Raman spectra of films with different Ta content, after standard vacuum annealing, are reported. Because of the very high intensity of the $E_g(1)$ peak with respect to all other peaks (see Figure 1), spectra are separated in two panels with arbitrary intensity units, in order to better appreciate the shape and relative intensities of the peaks (Figure 3 (a) and (b)). As the Ta content varies from 0% to 10%, some differences can be observed. First, a general decrease of the signal-to-noise ratio together

with a broadening of all peaks is evident, revealing an increasing disorder of the films with increasing Ta content, as expected from the substitution of Ti atoms with Ta atoms (Ta_{Ti}). Second, the $E_g(1)$ and $E_g(2)$ peaks shift towards higher frequencies with respect to their reference values of 144 and 197 cm^{-1}. **Figure 4** shows position and width (only for the most intense $E_g(1)$ mode) as a function of Ta content. A large variation of the peak position, from 144 to 158 cm^{-1}, is found, together with a significant broadening, from 10 to 24 cm^{-1}, as Ta content varies from 0% to 10%.

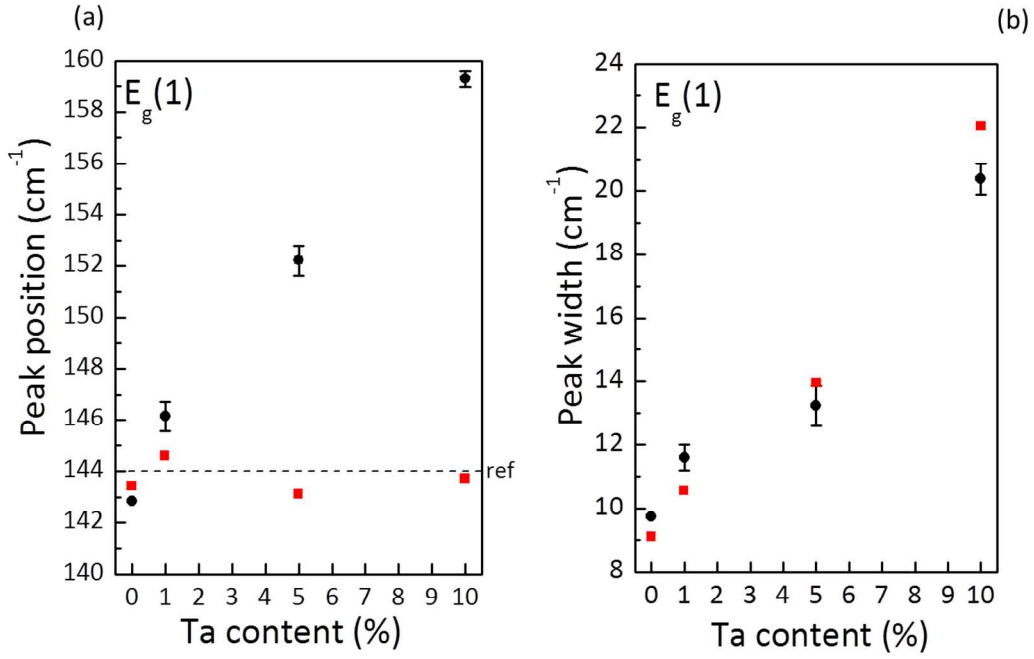

Figure 4. (a) Position and (b) width of the $E_g(1)$ peak, extracted from Lorentzian fit of the Raman spectra in Figure 3(a). Error bars refer to data from several samples at fixed preparation conditions. Black points refer to vacuum annealed films, red squares to air annealed films.

On the other hand, Raman spectra of twin samples annealed in air at similar temperature (550°C) show the $E_g(1)$ peak position always close to the reference value of 144 cm^{-1} regardless the Ta content (see Figure 3 (a)), while its width broadens in analogy with the vacuum annealed films (see fit data in

Figure 4 (b)). This observation qualitatively applies also to the $E_g(2)$ peak; nonetheless, due to the low intensity, a quantitative analysis of the $E_g(2)$ position and width is less accurate, and for this reason is not reported in this work. On the contrary, the other Raman peaks appear very similar to the ones of vacuum annealed films (both position and width). This is a very interesting and unexpected result, *i.e.* the amount of Ta, which is known to effectively substitute Ti regardless of the employed annealing atmosphere,[8,11,12,36] seems to affect both position and width of the $E_g(1)$ peak when vacuum annealing is performed. On the other hand, it only affects the peak width when oxygen is present in the annealing atmosphere. This suggests that the direct effect of Ta substitution in the Ti sublattice on the $E_g(1)$ peak is mainly a broadening effect, while the peak shift can be related to a more indirect effect. A possible explanation of this result will be provided later.

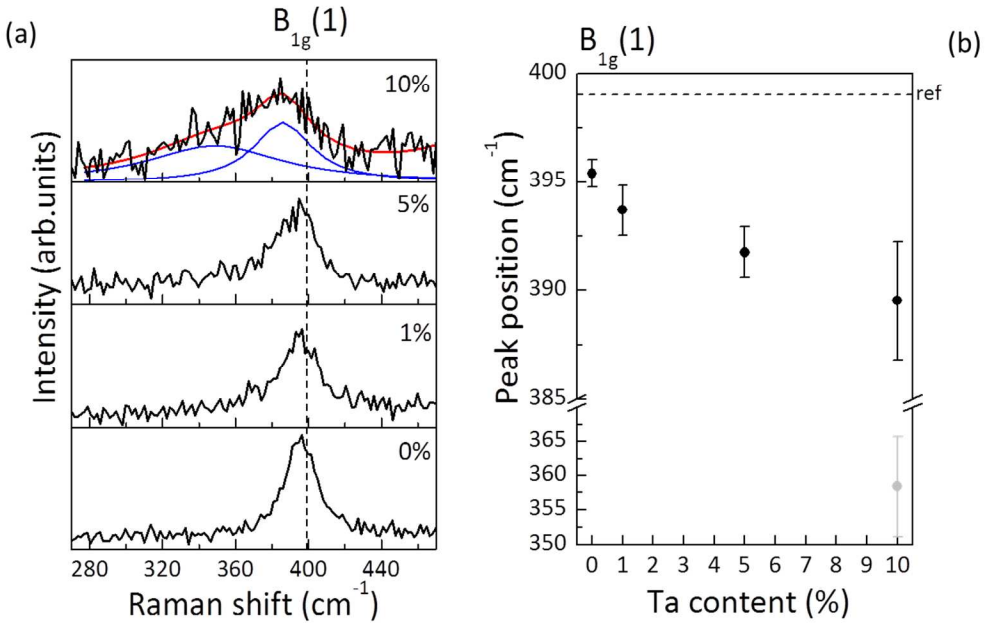

Figure 5. (a) $B_{1g}(1)$ Raman peak of Ta-doped TiO_2 films with different Ta content (0-10%) after vacuum annealing. The vertical line indicates reference peak position for anatase crystal. (b) Position of the $B_{1g}(1)$ peak, extracted from Lorentzian fit of the Raman spectra in (a). Error bars refer to data from

several samples at optimal preparation conditions. At 10% Ta content two peaks are necessary to fit the data, and the component at lower wavenumber is represented in gray.

Another important modification of the Raman spectrum depending on the Ta content concerns the $B_{1g}(1)$ mode (see **Figure 5** (a) and (b)). This mode is predicted to be dominated by Ti atom motions with negligible oxygen displacements,[20,21] hence it should be strongly sensitive to the presence of Ta_{Ti}. As the other peaks, it broadens at increasing Ta content. A detailed analysis shows that the $B_{1g}(1)$ mode always presents a small downshift (with a quite large variance of values (Figure 5 (b)); this is consistent with a more defected anatase lattice and in agreement with the corresponding phonon dispersion relation.[18] However, at high Ta content (10%) a change of the shape is evident with the appearance of a second component at lower frequencies (about 360 cm^{-1}), as shown in Figure 5 (a); a 2-peak Lorentzian fit gives good results in this case. To the best of our knowledge no Raman active modes in the proximity of the 360 cm^{-1} region could be reasonably assigned to different TiO_2 polymorphs or Ta-O-Ti-based phase segregations. Being this additional component just detected in the case of a large concentration of Ta_{Ti}, regardless the synthesis/annealing conditions, it is reasonable to hypothesize the activation of a Ta-Ti vibration inside the anatase crystal, whose significant shift towards lower frequencies with respect to the pure Ti-Ti vibration would be ascribed to the larger mass of Ta with respect to Ti.

Finally, the remaining Raman features, *i.e.* the composed mode $B_{1g}(2)$-A_{1g} and the $E_g(3)$ mode, show an increasing broadening with increasing Ta content, as visible in the spectra of Figure 3, with no significant trend in their position (confirmed by fit data, not shown here).

4.2 Effect of the oxygen deposition pressure

We have observed that the crystallization atmosphere is able to drastically change the electrical properties of TiO_2-based films from highly conducting to insulating (reducing vs. O-based atmosphere, respectively).[8,15] We also found that the oxygen pressure employed during the PLD process permits to finely tune the charge carrier density of vacuum annealed samples with a fixed extrinsic dopant concentration.

These results indicate that oxygen plays a fundamental role in the definition of electrical properties, probably with a delicate equilibrium between extrinsic dopant atoms, oxygen vacancies (which affect the charge carrier density especially in undoped samples[8,37]), and titanium vacancies and/or oxygen interstitials, acting as 'killer' defects for carriers.[12,14,38-40]

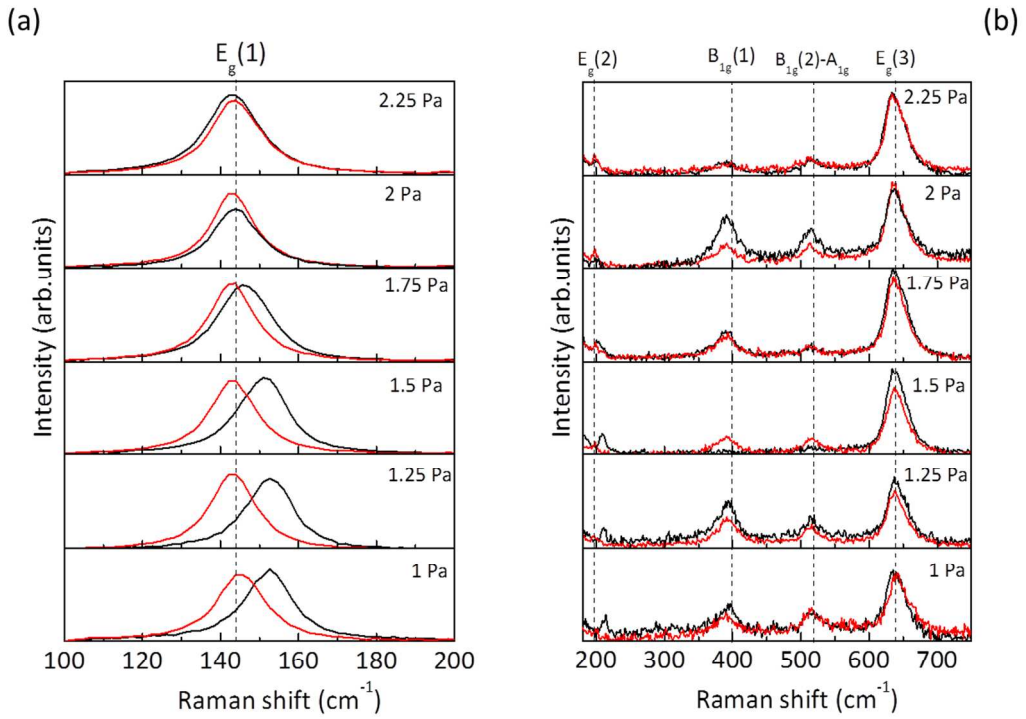

Figure 6. Raman spectra of Ta-doped TiO_2 films with fixed Ta content (5%) deposited at different oxygen pressure, after standard vacuum annealing (black lines) or air annealing (red lines). Vertical lines indicate reference peak position for anatase crystal.

In this framework, we present a Raman investigation on optimally doped TaTO films (Ta content = 5 at.%) deposited at different oxygen background PLD pressures (p_{O2} = 1 – 2.25 Pa). In **Figure 6** Raman spectra of films after standard vacuum or air annealing are reported. As a general observation, the shape of the peaks does not change in a significant way when varying oxygen deposition pressure in this range. On the other hand, the position of the two low frequency E_g peaks is not the same for all the vacuum annealed films. The effect is analogous for the two peaks, but much more clear for the more intense $E_g(1)$ peak (Figure 6 (a)), therefore we focus our discussion on it. Starting from the lower deposition pressure (1 Pa), the $E_g(1)$ peak appears to be significantly and strongly shifted towards higher frequencies with respect to the reference value of 144 cm^{-1}. This trend is confirmed at increasing p_{O2}, but with decreasing shifts, up to 2 Pa, for which the peak position coincides with the reference one.

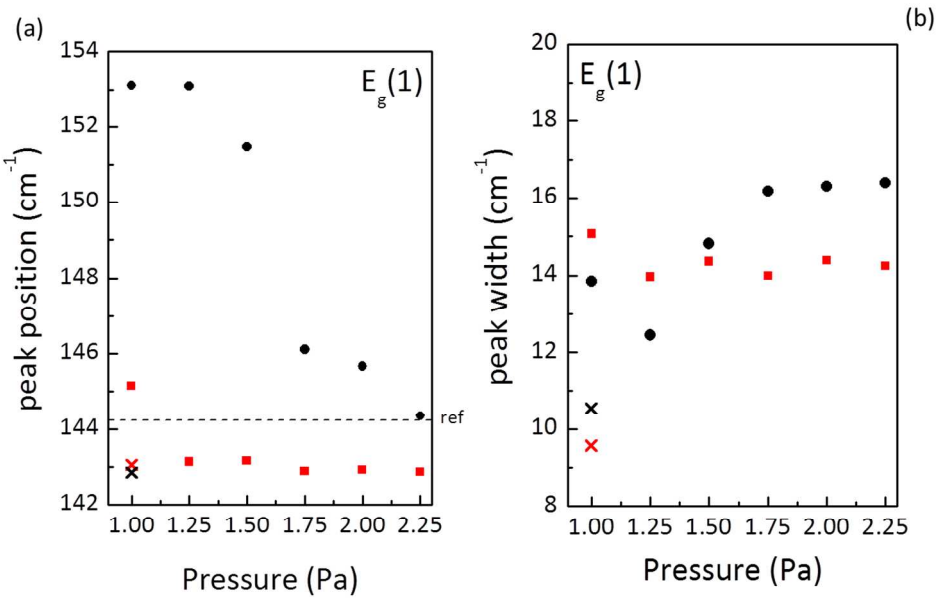

Figure 7. Black points: (a) Position and (b) width of the $E_g(1)$ peak, extracted from Lorentzian fit of the Raman spectra in fig.6 (vacuum annealed films, black curves). The red squares refer to twin films after annealing in air (red curves in fig.6). Crosses refer to undoped TiO_2, after annealing in vacuum (black) or in air (red). Raman spectra of Ta-doped TiO_2 films with fixed Ta content (5%) deposited at different oxygen.

A detailed analysis shows a variation of more than 10 cm^{-1} for $E_g(1)$ peak position in the investigated pressure range (see **Figure 7**). In air annealed films (see Figure 6 and 7), this behavior completely disappears and $E_g(1)$ positions always match the reference value. Regarding the $E_g(1)$ width, as reported in Figure 7 (b), a small variation with varying p_{O2} is found (14-17 cm^{-1}) for vacuum annealed samples, contrary to the broadening effect due to the Ta content discussed above; for air annealing the width variation is almost negligible. Thus, also in the case of films deposited at different O pressure, there appears to be no direct correlation between $E_g(1)$ peak position and width, and thus between peak position and structural disorder. We would like to observe that upon annealing in O-containing atmosphere (*i.e.* air) the width of the peaks does not change significantly with respect to vacuum annealing, both in the case of films with different Ta content and in films deposited at different oxygen pressure (see figs. 4(b), 6(b), 7(b)). This would be compatible with a non-significant amount of Ti vacancies created during the O-rich annealing. However, air annealing should also reduce O vacancies and induce O interstitials so that it is not easy to discern the factors affecting the width of Raman peaks. We finally note that, fixing Ta content, a variation of the $E_g(1)$ peak position is observed only when two conditions are satisfied simultaneously: the film is deposited at low p_{O2} (in the investigated range) and a reducing atmosphere is used during crystallization process. Moreover, if the variation is present, it is significant (up to 10 cm^{-1}), and always towards higher frequencies, in agreement with phonon dispersion relation.[18]

4.3 Charge carrier concentration – Raman shift relation

Different trends have been identified to depend on different material and deposition parameters (*i.e.* extrinsic dopant concentration, deposition p_{O2}, annealing atmosphere). In particular we have observed a

significant variation of the $E_g(1)$ and $E_g(2)$ peak positions both with Ta content and with deposition oxygen pressure, but only if a reducing atmosphere is used in the post-deposition annealing.

The same parameters are of paramount importance in determining the electrical properties of the material, which should be in turn related to the presence of a mixture of donor-like and 'killer' defects in the anatase lattice, and thus to the charge carrier density *n*.

Based on these considerations, we investigated the correlation between the position of the most intense $E_g(1)$ Raman peak and the measured charge carrier density of TiO_2-based films, obtained under different preparation conditions (the behavior of the $E_g(2)$ peak is analogous). To this purpose, a wide variety of conducting TiO_2-based samples have been analyzed via Raman spectroscopy, employing:

- different Ta content (0 – 1 – 5 – 10 at.%);
- different donor doping element (Nb-doped TiO_2 thin films deposited by sputtering have been considered in addition to PLD Ta-doped TiO_2 films);
- different p_{O2} (0.9-2.25 Pa) during the deposition process;
- different annealing cycles (standard cycle in vacuum or H_2-based atmosphere, ultra-fast-annealing in H_2- or N_2-based atmospheres - UFA).

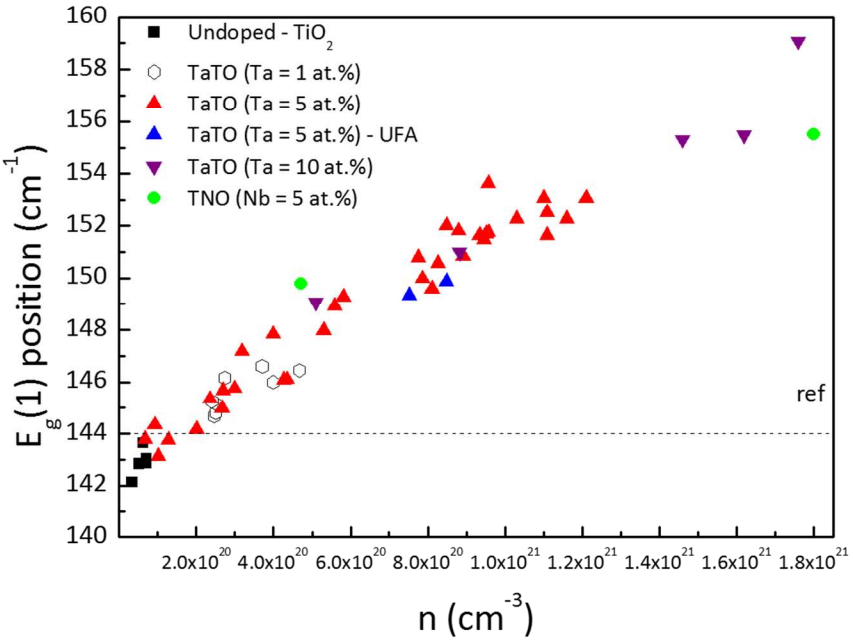

Figure 8. Raman peak position of the $E_g(1)$ anatase mode as a function of the measured charge carrier density.

In **Figure 8** the $E_g(1)$ Raman position is plotted as a function of the corresponding measured charge carrier density, revealing a clear relation between the two quantities, *i.e.* an increasing $E_g(1)$ position (from 144 to 160 cm^{-1}) with increasing *n* (from 10^{19} to 10^{21}, *i.e.* typical values for TCO materials). It is noteworthy to highlight that the evidenced trend is:

- independent of the amount of extrinsic doping;
- independent of the type of extrinsic dopant;
- independent of the annealing cycle and atmosphere (with the obvious strict condition of obtaining measurable electrical properties);

- almost linear for $n \leq 10^{21}$ cm^{-3}, while it seems to flatten for higher charge carrier concentrations (although more points should be collected in this region for a better statistics).

Understanding the origin of this relation is not trivial. Seeger *et al.* recently reported a similar trend with respect to carrier concentration for Nb-doped TiO_2,[41] invoking a distortion of the anatase structure due to the incorporation of niobium. However we observe no direct (unique) relationship between the anatase crystalline strain induced by dopant incorporation (see *e.g.* anatase lattice parameters for TaTO films reported in Figure 11 of ref.[8], corresponding to strains usually below ~0.005) and the $E_g(1)$ Raman peak shift. The extensive analysis here reported points to a more complex explanation and probably not directly related to the structural modifications induced by specific extrinsic and intrinsic defects. Nevertheless, this robust trend is connected in some ways to the possibility of finely tuning the amount of active dopants (or the equilibrium between donor-like and 'killer' defects) in TiO_2-based materials. A naïve/intuitive explanation could be based on the observation that the covalent bond strength, typical of metal oxides, could be increased by a partial 'metal-like' bonding due to conduction electrons, and leading to a significant hardening (and thus upshift) of the vibrational mode.

The peculiarity of the observed correlation stands in the almost linear trend (at least up to $n \sim 1\times10^{21}$ cm^{-3}) and in the entity of variation of more than 10 cm^{-1} (for higher n), much higher than the typical variation induced by other effects such as confinement, disorder and stoichiometry defects. The observed features remind a similar behavior observed in polar semiconductors, including III-V, II-VI and IV-IV compounds, based on the strong interaction between plasma oscillation of free carriers and phonons, with a formation of a LO phonon/plasmon coupled mode (LOPC).[42-47] The details of this interaction and its effects depend on many parameters, with different behavior for small- or wide-gap semiconductors and for different values of damping of the free carriers. In any case, the main effect is to shift the Raman peak corresponding to the LOPC mode. The entity of this variation can be very large, up to 200 cm^{-1} for densities of the order of 10^{19} cm^{-3}, while the particular trend depends on the material,

being linear for example for SiC,[44] but more rapid in semiconductors as GaN, where plasma frequency is comparable with phonon frequency, making the LOPC frequency more sensitive to *n*.[47] Our material is a wide-gap Ta/Nb-doped oxide, with a very large charge carrier density and relatively high electron effective mass for a TCO, leading to plasma wavelength of the order of 4000 nm, corresponding to a plasma frequency of about 2500 cm^{-1}, far from the frequency of the $E_g(1)$ peak (144 cm^{-1}).[8] Moreover, titanium oxide is not considered a polar material and no separation of LO and TO mode is observed. Nevertheless, a large degree of lattice defectivity could induce an increasing ionic character of the Ti-O bonds, besides a large charge carrier density value. With such high *n* and a partial polar character it is reasonable to suppose an interaction similar to the LOPC mode, but with lower values in the variation of the peak position and an even lower variation of the shape of the peak, almost not observable. This interpretative model would thus give account of the observed behavior, even though not quantitatively.

We here underline that this finding has not been reported before for conducting oxides, up to our knowledge; we also observe that the measured shift in the position of the $E_g(1)$ peak is in the same direction of the foreseen shift in the case of confinement or disorder effects, as dictated by the TiO_2 phonon dispersion relation;[18] this occurrence could possibly mask the 'electronic' effect, unless very large values of *n* are attained.

We finally note that the previous tentative explanation does not account for the different behavior of the various Raman peaks with respect to *n*, although the $E_g(2)$ mode behaves in a very similar way. Anyway a much higher sensitivity of the $E_g(1)$ peak to any disorder effect is extensively reported in the literature, probably related to a larger Raman cross section, making this peak the most intense (and narrow) among anatase Raman peaks. A more detailed theoretical model is needed to quantitatively explain this effect for the different vibrational modes. Apart from the exact interpretation of the physical phenomena behind the reported trend, it is noteworthy to underline the possibility to directly evaluate the charge carrier density in conductive TiO_2-based materials from a simple, quick,

nondestructive and contactless Raman analysis, independently from the dopant element employed and its amount.

5. Conclusions

Our results show that the Raman spectral features of polycrystalline TiO_2-based TCO films are strongly dependent on both the extrinsic dopant (Nb/Ta) concentration and the oxygen content, as determined by the deposition atmosphere or by the post-deposition annealing environment. We performed a systematic analysis of a wide variety of samples, discussing the observed effects on the shift and width of the main Raman peaks of the anatase structure.

The reported findings imply a non-obvious relationship between the material vibrational properties and its complex defect chemistry, involving e.g. substitutional dopant atoms, O vacancies, Ti vacancies, O interstitials and, possibly, defect complexes. Since the electrical conduction in this class of TCOs also depends on the film stoichiometry and on the preparation environment, it is clear that Raman spectroscopy represents a powerful tool to investigate the structure of TiO_2-based TCOs and the corresponding relation with the functional properties, especially if coupled with other complementary techniques. In particular, we reported a direct relationship between the charge carrier density and the Raman shift of the most intense $E_g(1)$ anatase peak, irrespective of the details of the different synthesis conditions or the specific structural properties. This relationship demonstrates a strong electron-phonon interaction in defected TiO_2, whose exact origin needs further investigation in order to achieve a satisfactory theoretical explanation. However, it can represent a tool for a quick, first evaluation of the charge carrier density in defected TiO_2 by Raman spectroscopy. We observe that a similar behavior could in principle be characteristic of other strongly doped TCOs and not observed so far.

Acknowledgments

A part of this work at KAST was supported by CREST, JST.

References:

1. Weng, Z.; Guo, H.; Liu, X.; Wu, S.; Yeung, K. W. K.; Chu, P.K. Nanostructured TiO_2 for Energy Conversion and Storage. *RSC Adv.* **2013**, *3*, 24758-24775.
2. Hanaor, D. A. H.; Sorrell C. C. Review of the Anatase to Rutile Phase Transformation. *J. Mat. Sci.* **2011**, *46*, 855-874.
3. Luttrell, T.; Halpegamage, S.; Tao, J.; Kramer, A.; Sutter, E.; Batzill, M. Why is Anatase a Better Photocatalyst than Rutile? - Model studies on epitaxial TiO_2 films. *Sci. Rep.* **2014**, *4,* 4043
4. Hagfeldt, A.; Boschloo, G.; Sun, L.; Kloo, L.; Pettersson, H. Dye-Sensitized Solar Cells. *Chem. Rev.* **2010**, *110*, 6595-6663.
5. Furubayashi, Y.; Hitosugi, T.; Yamamoto, Y.; Inaba, K.; Kinoda, G.; Hirose, Y.; Shimada, T.; Hasegawa, T. A Transparent Metal: Nb-doped Anatase TiO_2. *Appl. Phys. Lett.* **2005**, *86*, 252101.
6. Hitosugi, T.; Furubayashi, Y.; Ueda, A.; Itabashi, K.; Inaba, K.; Hirose, Y.; Kinoda, G.; Yamamoto, Y.; Shimada, T.; Hasegawa, T. Ta-doped Anatase TiO_2 Epitaxial Film as Transparent Conducting Oxide. *Jpn. J. Appl. Phys. 2* **2005**, *44*, L1063-L1065.
7. Hitosugi, T.; Yamada, N.; Nakao, S.; Hirose, Y.; Hasegawa, T. Properties of TiO_2-based Transparent Conducting Oxides. *Phys. Status Solidi A* **2010**, *207*, 1529-1537.
8. Mazzolini, P.; Gondoni, P.; Russo, V.; Chrastina, D.; Casari, C. S.; Li Bassi, A. Tuning of Electrical and Optical Properties of Highly Conducting and Transparent Ta-Doped TiO_2 Polycrystalline Films. *J. Phys. Chem. C* **2015**, *119*, 6988-6997

9. Lee, H.-Y.; J. Robertson. Doping and Compensation in Nb-doped Anatase and Rutile TiO_2. *J. Appl. Phys.* **2013**, *113*, 213706

10. Ok, K.-C.; Park, Y.; Chung, K.-B.; Park, J.-S. The Effect of Ta Doping in Polycrystalline TiO_x and the Associated Thin Film Transistor Properties. *Appl. Phys. Lett.* **2013**, *103*, 213501

11. Osorio-Guillén, J., Lany, S.; Zunger, A. Atomic Control of Conductivity Versus Ferromagnetism in Wide-Gap Oxides Via Selective Doping: V, Nb, Ta in Anatase TiO_2. *Phys. Rev. Lett.* **2008**, *100*, 036601

12. Rusydi, A.; Dhar, S.; Roy Barman, A.; Riando, A.; Qi, D.-C.; Motapothula, M.; Yi, J. B.; Santoso, I.; Feng, Y. P.; Yang, K., et al. Cationic-vacancy-induced Room-Temperature Ferromagnetism in Transparent Conducting Anatase $Ti_{1-x}Ta_xO_2$ (x~0.05) Thin Films. *Phil Trans. R. Soc. A* **2012**, *370*, 4927-4943

13. Yamamoto, T.; Ohno T. Screened Hybrid Density Functional Study on Nb- and Ta-doped TiO_2. *Phys. Rev. B* **2012**, *85*, 013304

14. Qi, D.C.; Barman, A. R.; Debbichi, L.; Dhar, S.; Santoso, I.; Asmara, T. C.; Omer, H.; Yang, K.; Krüger, P.; Wee, A. T. S., et al. Cationic Vacancies and Anomalous Spectral-Weight Transfer in $Ti_{1-x}Ta_xO_2$ Thin Films studied via Polarization-dependent Near-Edge x-ray Absorption Fine Structure Spectroscopy. *Phys. Rev. B* **2013**, *87*, 245201

15. Mazzolini, P.; Acartürk., T.; Chrastina, D.; Starke, U.; Casari, C. S.; Gregori, G.; Li Bassi, A. Controlling the Electrical Properties of Undoped and Ta-Doped TiO2 Polycrystalline Films via Ultra-Fast-Annealing Treatments. *Adv. Electron. Mat.* **2016**, *2*, 1500316

16. Russo, V.; Ghidelli, M.; Gondoni, P.; Casari, C. S.; Li Bassi, A. Multi-Wavelength Raman Scattering of Nanostructured Al-Doped Zinc Oxide. *J. Appl. Phys.* **2014**, *115*, 073508

17. LiBassi, A.; Cattaneo, D.; Russo, V.; Bottani, C. E.; Barborini, E.; Mazza, T.; Piseri, P.; Milani, P.; Ernst, F. O.; Wegner, K., et al. Raman Spectroscopy Characterization of Titania Nanoparticles

Produced by Flame Pyrolysis: The Influence of Size and Stoichiometry. *J. Appl. Phys*. **2005**, *98*, 074305

18. Mikami, M.; Nakamura, S.; Kitao, O.; Arakawa, H. Lattice Dynamics and Dielectric Properties of TiO_2 Anatase: A First-Principles Study. *Phys. Rev. B* **2002**, *66*, 155213
19. Oshaka, T.; Izumi, F.; Fujiiki, Y. Raman Spectrum of Anatase, TiO_2. *J. Raman Spectrosc.* **1978**, *7*, 321-324
20. Frank, O.; Zukalova, M.; Laskova, B.; Kurti, J.; Koltai, J.; Kavan, L. Raman Spectra of Titanium Dioxide (Anatase, Rutile) with Identified Oxygen Isotopes (16, 17, 18). *Phys. Chem. Chem. Phys.* **2012**, *14*, 14567-14572
21. Kavan, L.; Zukalova, M.; Ferus, M.; Kurti, J.; Koltai, J.; Civis, S. Oxygen-Isotope Labeled Titania: $Ti^{18}O_2$. *Phys. Chem. Chem. Phys.* **2011**, *13*, 11583-11586
22. Giarola, M.; Sanson, A.; Monti, F.; Mariotto, G.; Bettinelli, M.; Speghini, A.; Salviulo, G. Vibrational Dynamics of Anatase TiO_2: Polarized Raman Spectroscopy and *ab initio* Calculations. *Phys. Rev. B* **2010**, *81*, 174305
23. Balachandran, U.; Eror, N.G. Raman Spectra of Titanium Dioxide. *J. Solid State Chem.* **1982**, *42*, 276-282
24. Parker, J.C.; Siegel R.W. Calibration of the Raman Spectrum to the Oxygen Stoichiometry of Nanophase TiO_2. *Appl. Phys. Lett.* **1990**, *57*, 943-945
25. Sahoo, S.; Arora A.K.; Sridharan, V. Raman Line Shapes of Optical Phonons of Different Symmetries in Anatase TiO_2 Nanocrystals. *J. Phys. Chem. C* **2009**, *113*, 16927-16933
26. Bersani, D.; Lottici P.P.; Ding X.-Z. Phonon Confinement Effects in the Raman Scattering by TiO_2 Nanocrystals. *App. Phys. Lett.* **1998**, *72*, 73-75

27. Barborini, E.; Kohlmanov, I. N.; Piseri, P.; Ducati, C.; Bottani, C. E.; Milani, P. Engineering the Nanocrystalline Structure of TiO_2 Films by Aerodynamically Filtered Cluster Deposition. *App. Phys. Lett.* **2002**, *81*, 3052-3054

28. Lejon, C.; Österlund, L. Influence of Phonon Confinement, Surface Stress, and Zirconium Doping on the Raman Vibrational Properties of Anatase TiO_2 Nanoparticles. *J. Raman Spectrosc.* **2011**, *42*, 2026-2035

29. Choudhury, B.; Dey M.; Choudhury A. Defect Generation, d-d Transition, and Band Gap Reduction in Cu-Doped TiO_2 Nanoparticles. *Int. Nano Lett.***2013**, *3*,1-8

30. Navas, J.; Sanchez-Coronilla, A.; Aguilar, T.; Hernandez, N. J.; de los Santos, D. M.; Sanchez-Marquez, J.; Zorrilla, D.; Fernandez-Lorenzo, C.; Alcantara, R.; Martın-Calleja, J. Experimental and Theoretical Study of the Electronic Properties of Cu-Doped Anatase TiO_2. *Phys. Chem. Chem. Phys.* **2014**, *16*, 3835-3845

31. Ruiz, A. M.; Dezanneau, G.; Arbiol, J.; Cornet, A.; Morante, J. R. Insights into the Structural and Chemical Modifications of Nb Additive on TiO_2 Nanoparticles. *Chem. Mat.* **2004**, *16*, 862-871

32. Ščepanovic, M.; Askrabic, S.; Berec, V.; A. Golubovi, A.; Dohcevic-Mitrovic, Z.; Kremenovic, A.; Popovic, Z. V. Characterization of La-Doped TiO_2 Nanopowders by Raman Spectroscopy. *Acta Phys. Pol. A* **2009**, *115*, 771-774

33. Castro, M.V; Rebouta, L.; Alpuima, P.; Cerqueira , M. F.; Benelmekki, M.; Garcia, C. B.; Alves, E.; Barradas, N. P.;, Xuriguera, E.; Tavares, C. J. Optimization of Surface Treatments of TiO_2:Nb Transparent Conductive Coatings by a Post-hot-wire Annealing in a Reducing H_2 Atmosphere. *Thin Solid Films* **2014**, *550*, 404-412

34. Hearne, G.R.; Zhao, J.; Dawe, A. M.; Pischedda, V.; Maaza, M.; Nieuwoudt, M. K.; Kibasomba, P.; Nemraoui, O.; Comins, J. D.; Witcomb. M. J. Effect of Grain Size on Structural Transitions in Anatase TiO_2: A Raman Spectroscopy Study at High Pressure. *Phys. Rev. B* **2004**, *70*, 134102

35. Alhomoudi, I.A.; Newaz G. Residual Stresses and Raman Shift Relation in Anatase TiO_2 Thin Film. *Thin Solid Films* **2009**, *517*, 4372-4378

36. Neubert, M.; Cornelius, S.; Fiedler, J.; Gebel, T.; Liepack, H.; Kolitsch, A.; Vinnichenko, M. Overcoming Challenges to the Formation of High-Quality Polycrystalline TiO_2:Ta Transparent Conducting Films by Magnetron Sputtering. *J. Appl. Phys.* **2013**, *114*, 083707

37. Deák, P.; Aradi B.; Frauenheim T. Quantitative Theory of the Oxygen Vacancy and Carrier Self-Trapping in bulk TiO_2. *Phys. Rev. B* **2012**, *86*, 195206

38. Nowotny, J.; Bak, T.; Nowotny, M. K.; Sheppard, L. R. Defect Chemistry and Electrical Properties of Titanium Dioxide. 1. Defect Diagrams. *J. Phys. Chem. C* **2007**, *112*, 590-601

39. Morgan, B. J.; Watson, G.W. Polaronic Trapping of Electrons and Holes by Native Defects in Anatase TiO_2. *Phys. Rev. B* **2009**, *80*, 233102

40. Kamisaka, H; Hitosugi, T.; Suenaga, T.; Hasegawa, T.; Yamashita, K. Density Functional Theory Based First-Principle Calculation of Nb-Doped Anatase TiO_2 and Its Interactions with Oxygen Vacancies and Interstitial Oxygen, *J. Chem. Phys.* **2009**, *131*, 034702

41. Seeger, S.; Ellmer, K.; Weise, M.; Gogova, D.; Abou-Ras, D.; Mientus, R. Reactive Magnetron Sputtering of Nb-Doped TiO2 Films: Relationships between Structure, Composition and Electrical Properties. *Thin Solid Films* **2015**, *605*, 44-52

42. Varga, B. B. Coupling of Plasmons to Polar Phonons in Degenerate Semiconductors. *Phys. Rev* **1965**, *137*, A1896-1902.

43. Mooradian, A.; Wright, G. B. Observation of the Interaction of Plasmons with Longitudinal Optical Phonons in GaAs. *Phys. Rev. Lett*. **1966**, *16*, 999-1001.

44. Nakashima, S.; Kitamura, T.; Mitani, T.; Okumura H.; Katsuno, M.; Ohtani, N. Raman Scattering Study of Carrier-Transport and Phonon Properties of 4H -SiC Crystals with Graded Doping. *Phys. Rev. B* **2007**, *76*, 245208

45. Cuscó, R.; Artus, L.; Hernandez, S.; J. Ibanez, J.; Hopkinson, M. Raman Scattering by LO Phonon-Plasmon Coupled Modes in n-type $In_{0.53}Ga_{0.47}As$. *Phys. Rev. B* **2001**, *65*, 035210

46. Kozawa, T.; Kachi, T.; Kano, H.; Taga, Y.; Hashimoto, M.; Koide, N.; Manabe, K. Raman Scattering from LO Phonon-Plasmon Coupled Modes in Gallium Nitride. *J. Appl. Phys.* **1994**, *75*, 1098-1101

47. Wetzel, C.; Walukiewicz, W.; Haller, E. E.; Ager, J. Carrier Localization of As-Grown n-Type Gallium Nitride under Large Hydrostatic Pressure. *Phys. Rev. B* **1996**, *53*, 1322-1326

TOC graphic

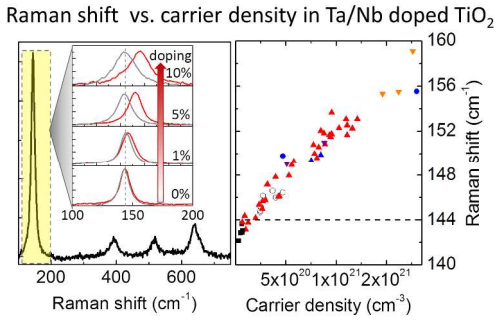
Raman shift vs. carrier density in Ta/Nb doped TiO2
doping
10%
5%
1%
0%
100
150
200
200
400
600
Raman shift (cm-1)
160
156
152
148
144
140
Raman shift (cm-1)
5x10^20
1x10^21
2x10^21
Carrier density (cm-3)

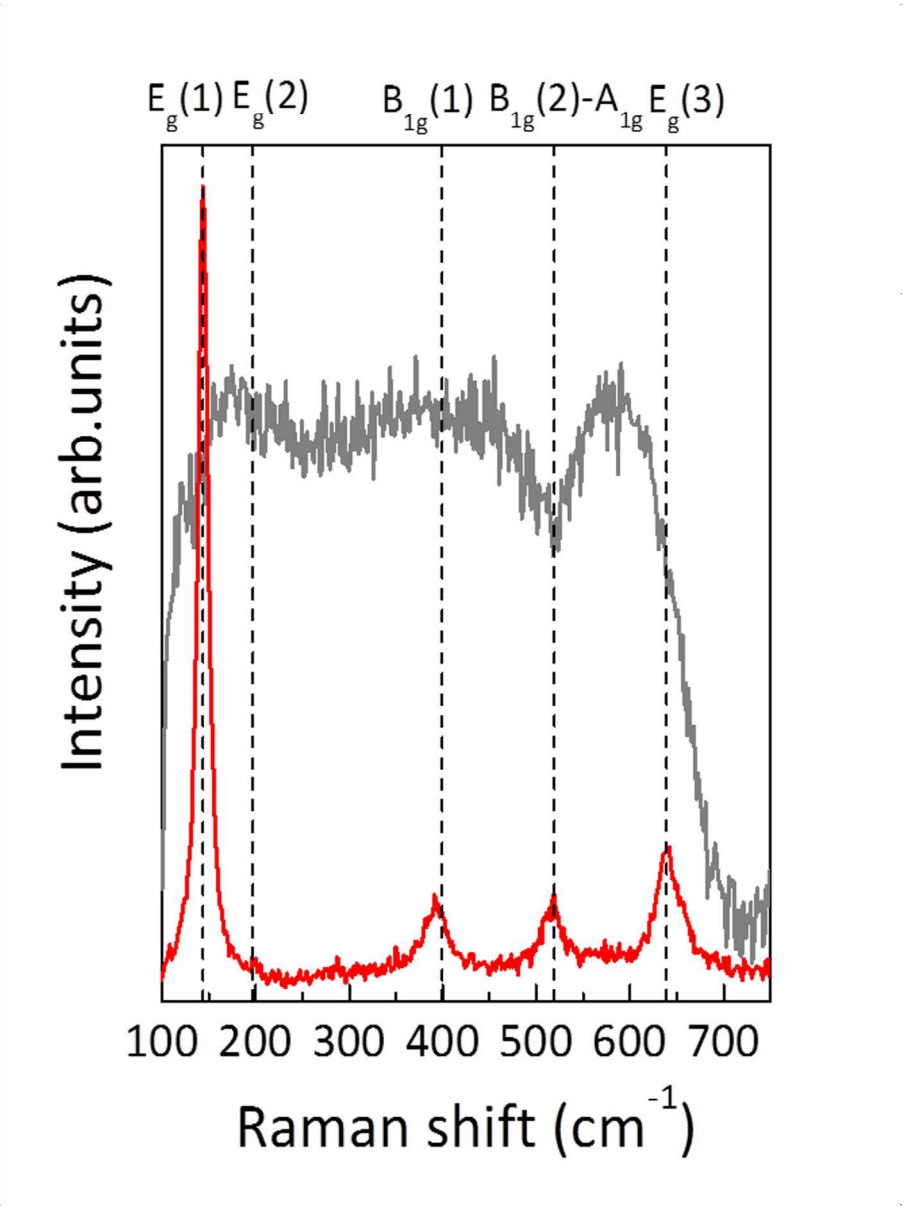

Figure 1. Raman spectra obtained for a film as deposited (with 1.25 Pa O_2) (grey curve) and after annealing in air at 550°C (red curve)
Figure 1
270x360mm (150 x 150 DPI)

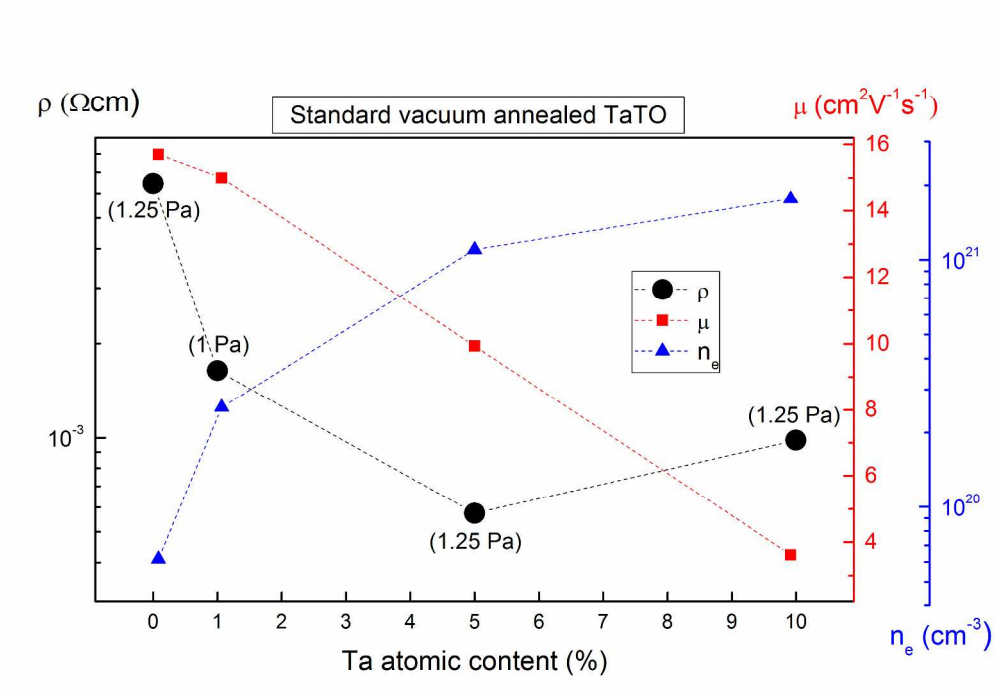

Figure 2. Best electrical properties obtained for standard vacuum annealed polycrystalline TaTO films as a function of different Ta content. The black circles represent the resistivity *ρ*, the blue triangles the charge carrier density *n* and the red squares the electron mobility *μ*. In the brackets the oxygen partial pressure employed during the previous room temperature deposition process is reported.

Figure 2
288x201mm (300 x 300 DPI)

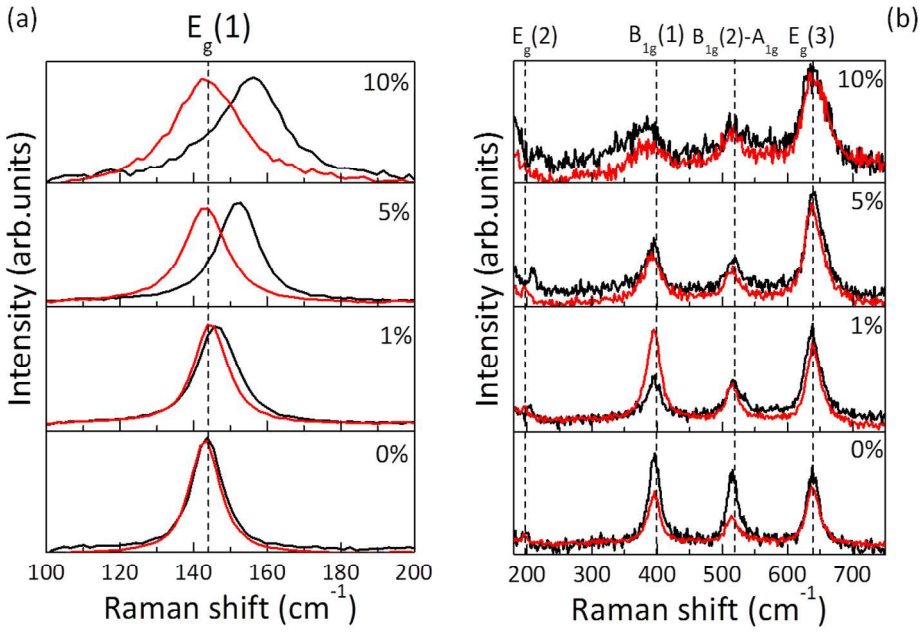

Figure 3. Raman spectra of TaTO films with different Ta content after standard vacuum annealing (black curves) or air annealing at 500°C (red curves). Vertical lines indicate reference peak position for anatase crystal.

Figure 3
406x282mm (150 x 150 DPI)

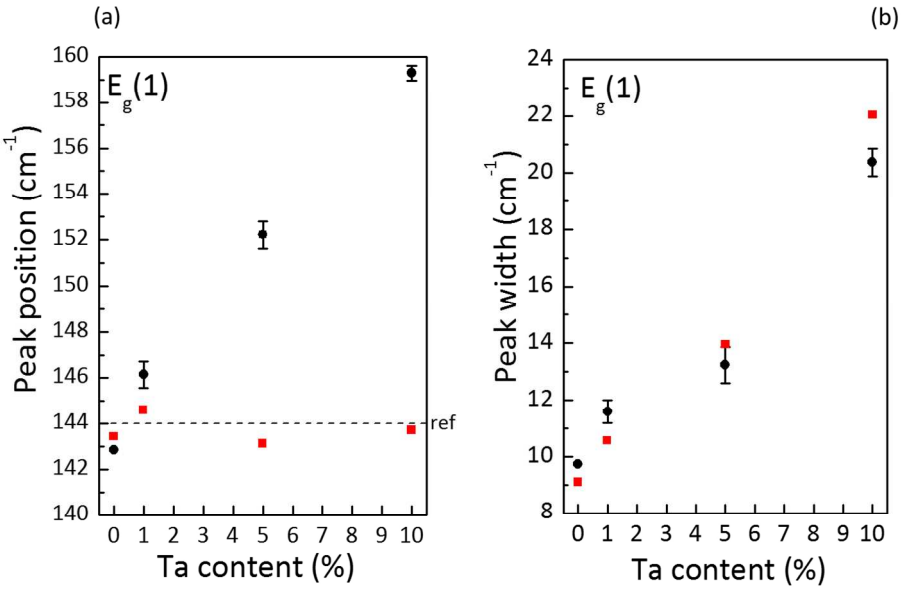

Figure 4. (a) Position and (b) width of the $E_g(1)$ peak, extracted from Lorentzian fit of the Raman spectra in Figure 3(a). Error bars refer to data from several samples at fixed preparation conditions. Black points refer to vacuum annealed films, red squares to air annealed films.

Figure 4
406x257mm (150 x 150 DPI)

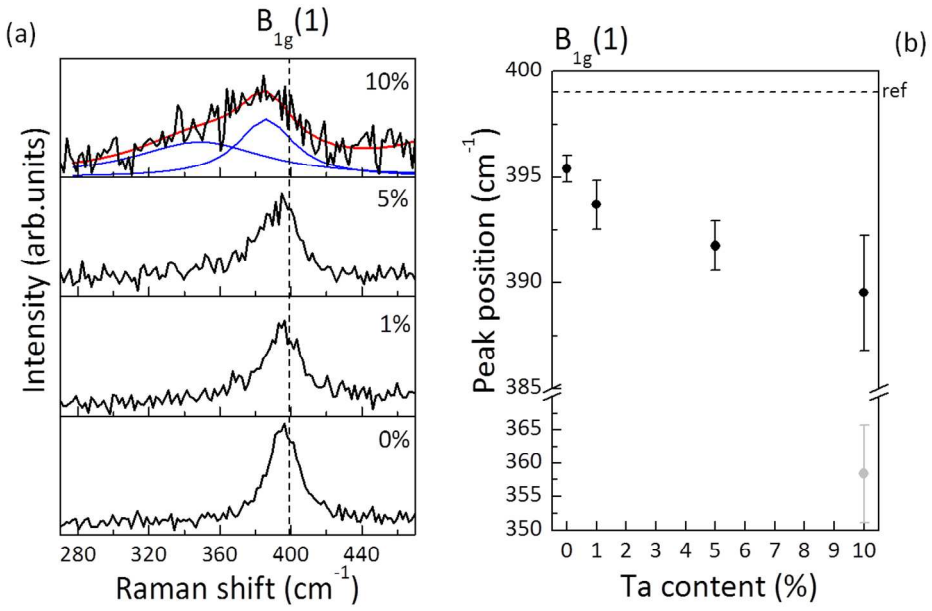

Figure 5. (a) $B_{1g}(1)$ Raman peak of Ta-doped TiO_2 films with different Ta content (0-10%) after vacuum annealing. The vertical line indicates reference peak position for anatase crystal. (b) Position of the $B_{1g}(1)$ peak, extracted from Lorentzian fit of the Raman spectra in (a). Error bars refer to data from several samples at optimal preparation conditions. At 10% Ta content two peaks are necessary to fit the data, and the component at lower wavenumber is represented in gray.

Figure 5
406x272mm (150 x 150 DPI)

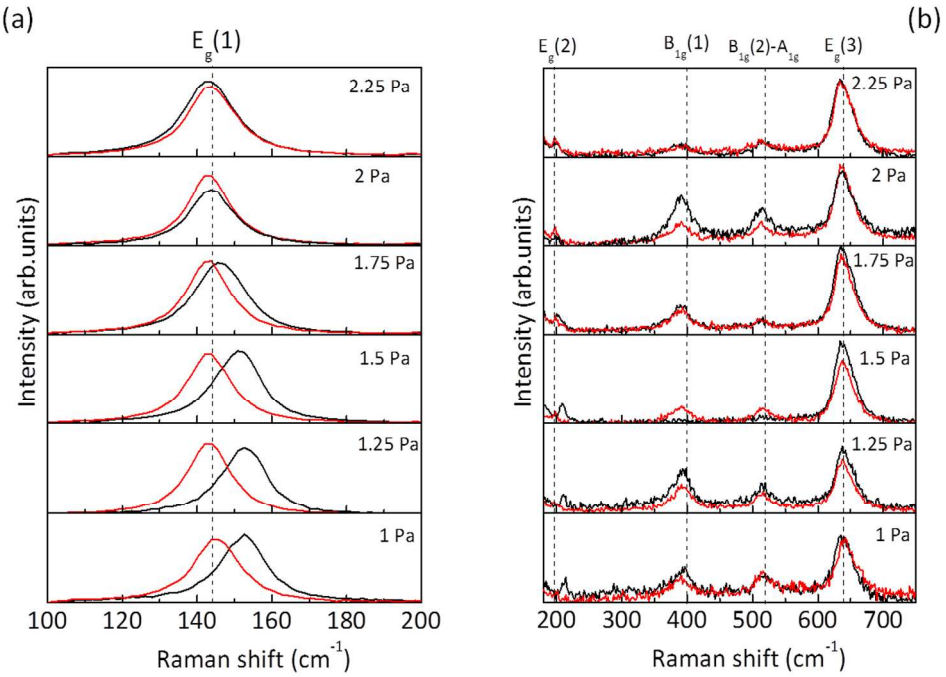

Figure 6. Raman spectra of Ta-doped TiO_2 films with fixed Ta content (5%) deposited at different oxygen pressure, after standard vacuum annealing (black lines) or air annealing (red lines). Vertical lines indicate reference peak position for anatase crystal.

Figure 6
406x295mm (150 x 150 DPI)

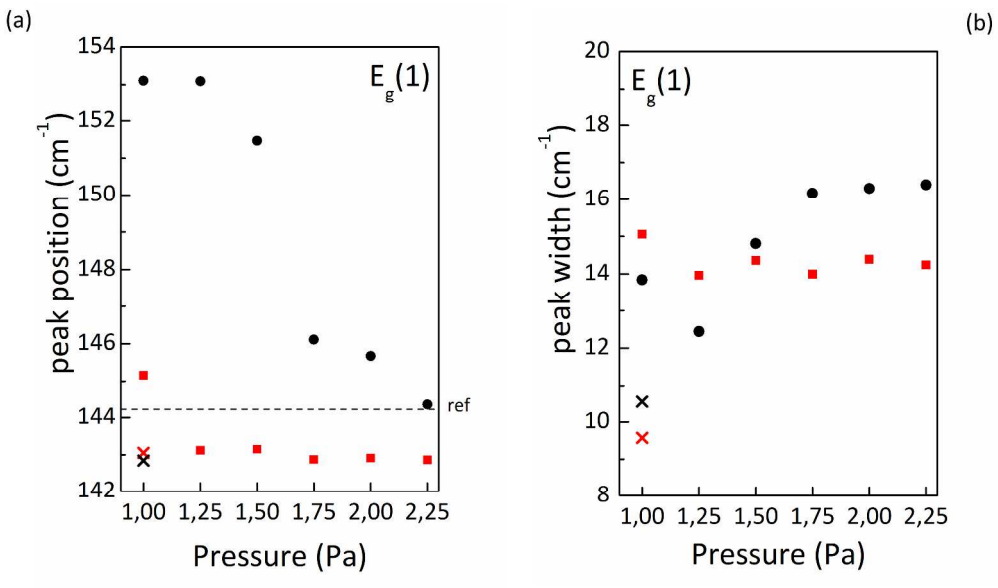

Figure 7. Black points: (a) Position and (b) width of the $E_g(1)$ peak, extracted from Lorentzian fit of the Raman spectra in fig.6 (vacuum annealed films, black curves). The red squares refer to twin films after annealing in air (red curves in fig.6). Crosses refer to undoped TiO_2, after annealing in vacuum (black) or in air (red). Raman spectra of Ta-doped TiO_2 films with fixed Ta content (5%) deposited at different oxygen.
Figure 7
1023x599mm (96 x 96 DPI)

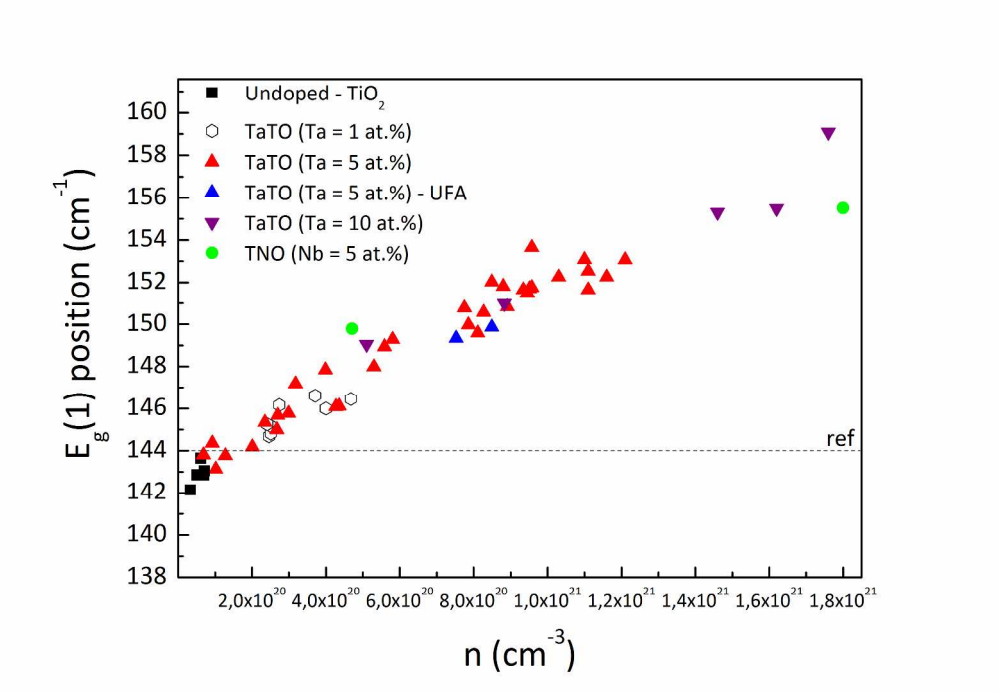

Figure 8. Raman peak position of the $E_g(1)$ anatase mode as a function of the measured charge carrier density.
Figure 8
290x201mm (300 x 300 DPI)